THE EUROPEAN
PHYSICAL JOURNAL C

Real-time cosmology with SKA

Yan Liu[1]**, Jing-Fei Zhang**[1]**, Xin Zhang**[1,2,3,a]

[1] Department of Physics, College of Sciences, Northeastern University, Shenyang 110819, China
[2] Ministry of Education's Key Laboratory of Data Analytics and Optimization for Smart Industry, Northeastern University, Shenyang 110819, China
[3] Center for High Energy Physics, Peking University, Beijing 100080, China

Abstract In this work, we investigate what role the redshift-drift data of the Square Kilometre Array (SKA) will play in the cosmological parameter estimation in the future. To test the constraint capability of the redshift-drift data of SKA-only, the ΛCDM model is chosen as a reference model. We find that using the SKA1 mock data, the ΛCDM model can be loosely constrained, while the model can be well constrained when the SKA2 mock data are used. When the mock data of SKA are combined with the data of the European Extremely Large Telescope (E-ELT), the constraints can be significantly improved, becoming almost as good as the data combination of the type Ia supernovae observation (SN), the cosmic microwave background observation (CMB), and the baryon acoustic oscillations observation (BAO). Furthermore, we explore the impact of the redshift-drift data of SKA on the basis of SN+CMB+BAO+E-ELT in the ΛCDM model, the wCDM model, the CPL model, and the HDE model. We find that the redshift-drift measurement of SKA could help to significantly improve the constraints on dark energy and could break the degeneracy between the cosmological parameters. Therefore, we conclude that redshift-drift observation of SKA would provide a good improvement in the cosmological parameter estimation in the future and has the enormous potential to be one of the most competitive cosmological probes in constraining dark energy.

1 Introduction

The accelerated expansion of the universe has been discovered and confirmed by cosmological observations for about 20 years, which is undoubtedly one of the greatest scientific discoveries in modern cosmology. However, the science behind the cosmic acceleration, i.e., the nature of dark energy, still remains mysterious. To measure the physical property

of dark energy, one should precisely measure the expansion history of the universe. Currently, the mainstream way is to measure the cosmic distances (luminosity distance or angular diameter distance) and the corresponding redshifts, and to establish a distance–redshift relation, by which constraints on the parameters of dark energy (and other cosmological parameters) can be made. However, a more straightforward way is to directly measure the expansion rate of the universe at different redshifts, although this measurement is more difficult in the observational cosmology.

With the fast advancement in technology over the past several decades, the possibility of measuring the temporal variation of astrophysical observable quantities over a few decades is becoming more and more realistic. This kind of real-time observations can be called "real-time cosmology". The most typical real-time observable is the redshift drift, which can give a direct measurement for the expansion rate (namely, the Hubble parameter) of the universe in a specific range of redshift.

The approach of measuring the redshift drift was first proposed by Sandage, who suggested a direct measurement of the redshift variation for the extra-galactic sources [1]. At the time he wrote, obviously, such a measurement was out of reach with the technological limitation of the day. Then the method was further improved by Loeb, who suggested a more realistic way of measuring the redshift drift using Lyman-α absorption lines of the distant quasars (QSOs) to detect the redshift variation [2]. Loeb concluded that the signal would be detectable when 100 quasars can be observed over 10 years with a 10-m class telescope. Thus, the method of redshift-drift measurement is also referred to as the "Sandage–Loeb" (SL) test.

Based on SL test, the scheduled European Extremely Large Telescope (E-ELT), a giant 40-m class optical telescope, is equiped with a high-resolution spectrograph to perform the COsmic Dynamics EXperiment (CODEX). The

---

[a] e-mail: zhangxin@mail.neu.edu.cn (corresponding author)

experiment is designed to detect the SL-test signals by observing the Lyman-α absorption lines within the redshift range of $2 \lesssim z \lesssim 5$. The forecast of using the redshift drift from the E-ELT to constrain dark energy models has been extensively discussed; see, e.g., Refs. [3–18]. It has been shown that the redshift drift in the redshift range of $2 < z < 5$ is rather useful to break the parameter degeneracies generated by other observations and thus can play an important role in the cosmological parameter estimation in the future.

The Square Kilometre Array (SKA) will soon start construction for the Phase one. Actually, SKA can also perform the research of real-time cosmology. Instead of detecting the Lyman-α absorption lines of the quasar, SKA will measure the spectral drift in the neutral hydrogen (HI) emission signals of galaxies to implement the measurement of redshift drift in the redshift range of $0 < z < 1$. Obviously, the redshift-drift data of SKA provide an important supplement to those of E-ELT.

In this work, we will study the real-time cosmology with the redshift-drift observation from SKA. We will simulate the redshift-drift data of SKA and use these data to constrain cosmological parameters. We have the following aims in this work: (i) We wish to learn what extent the cosmological parameters can be constrained to by using the redshift-drift data of SKA-only. (ii) We wish to learn what will happen when the redshift-drift data of SKA and E-ELT are combined to perform constraints on cosmological parameters. (iii) We wish to learn what role the redshift-drift data of SKA will play in the cosmological parameter estimation in the future.

We will employ several typical and simple dark energy models to perform the analysis of this work. We will consider the Λ cold dark matter (ΛCDM) model in this work, which is the simplest cosmological model and is able to explain the various current cosmological observations quite well. The wCDM model is the simplest extension to the ΛCDM model, in which the equation-of-state (EoS) parameter w of dark energy is assumed to be a constant. The Chevalliear–Polarski–Linder (CPL) [19,20] model of dark energy is a further extension to the ΛCDM model, in which the form of $w(a) = w_0 + w_a(1 - a)$, with the two free parameters w_0 and w_a, is proposed to describe the cosmological evolution of the EoS of dark energy. We will also consider the holographic dark energy (HDE) model [21] in this work, which is a dynamical dark energy model based on the consideration of quantum effective field theory and the holographic principle of quantum gravity [22]. In the HDE model, the type (quintessence or quintom) and the cosmological evolution of dark energy are solely determined by a dimensionless constant c (note that this is not the speed of light) [23]. For more detailed studies on the HDE model, see e.g. Refs. [11,13,22–46]. In this work, we use these four typical, simple dark energy models, namely, the ΛCDM, wCDM, CPL,

and HDE models, as examples to make an analysis for the real-time cosmology.

The structure of this paper is arranged as follows. In Sect. 2, we present the analysis method and the observational data used in this work. In Sect. 3, we report the constraint results of cosmological parameters and make some relevant discussions. In Sect. 4, the conclusion of this work is given.

2 Method and data

We will simulate the redshift-drift data of SKA, and use these mock data to constrain the cosmological models. We will also simulate the redshift-drift data of E-ELT, and make a comparison and combination with the data of SKA. In order to check how the redshift-drift data of SKA will break the parameter degeneracies generated by other cosmological observations, we will also consider the current mainstream observations in this work.

2.1 A brief description of the dark energy models

In this subsection, we will briefly describe the dark energy models employed in the analysis of this work. In a spatially flat universe with a dark energy having an EoS $w(z)$, the form of the Hubble expansion rate is given by the Friedmann equation,

$$E^2(z) \equiv \frac{H^2(z)}{H_0^2} = \Omega_{\rm m}(1 + z)^3 + \Omega_{\rm r}(1 + z)^4$$
$$+ (1 - \Omega_{\rm m} - \Omega_{\rm r}) \exp\left(3 \int_0^z \frac{1 + w(z')}{1 + z'} {\rm d}z'\right), \tag{1}$$

where $\Omega_{\rm m}$ and $\Omega_{\rm r}$ correspond to the present-day fractional densities of matter and radiation, respectively. Next, we will directly give the expressions of $E(z)$ for the ΛCDM, wCDM, CPL, and HDE models. Note that, since we mainly focus on the evolution of the late universe, in the following we shall neglect the radiation component.

- ΛCDM model: Since the cosmological constant Λ can explain the various cosmological observations quite well, it has nowadays become the preferred and simplest candidate for dark energy, although it has been suffering from severe theoretical puzzles. The EoS of the cosmological constant is $w = -1$, and thus we have

$$E^2(z) = \Omega_{\rm m}(1 + z)^3 + (1 - \Omega_{\rm m}). \tag{2}$$

- wCDM model: In this model, the EoS of dark energy is assumed to be a constant, i.e., $w = {\rm constant}$, and thus it is the simplest case for the dynamical dark energy. For

this model, the expression of $E(z)$ is given by

$$E^2(z) = \Omega_{\rm m}(1 + z)^3 + (1 - \Omega_{\rm m})(1 + z)^{3(1+w)}. \qquad (3)$$

- CPL model: In this model, the form of the EoS of dark energy $w(a)$ is parameterized as $w(a) = w_0 + w_a(1-a)$, with the two free parameters w_0 and w_a. Thus, we have

$$E^2(z) = \Omega_{\rm m}(1 + z)^3 + (1 - \Omega_{\rm m}) \\ \times (1 + z)^{3(1+w_0+w_a)} \exp\left(-\frac{3w_a z}{1+z}\right). \qquad (4)$$

- HDE model: In this model, the dark energy density is assumed to be of the form $\rho_{\rm de} = 3c^2 M_{\rm pl}^2 R_{\rm eh}^{-2}$ [22], where c is a dimensionless parameter, $M_{\rm pl}$ is the reduced Planck mass, and $R_{\rm eh}$ is the future event horizon defined as $R_{\rm eh}(t) = a r_{\rm max}(t) = a(t)\int_t^\infty {\rm d}t'/a(t')$. The evolution of the universe in this model is determined by the following two differential equations:

$$\frac{1}{E(z)}\frac{{\rm d}E(z)}{{\rm d}z} = -\frac{\Omega_{\rm de}(z)}{1+z}\left(\frac{1}{2} + \frac{\sqrt{\Omega_{\rm de}(z)}}{c} - \frac{3}{2\Omega_{\rm de}(z)}\right), \qquad (5)$$

$$\frac{{\rm d}\Omega_{\rm de}(z)}{{\rm d}z} = -\frac{2\Omega_{\rm de}(z)(1 - \Omega_{\rm de}(z))}{1+z}\left(\frac{1}{2} + \frac{\sqrt{\Omega_{\rm de}(z)}}{c}\right). \qquad (6)$$

Numerically solving the two differential equations with the initial conditions $E(0) = 1$ and $\Omega_{\rm de}(0) = 1 - \Omega_{\rm m}$ will directly give the evolutions of $E(z)$ and $\Omega_{\rm de}(z)$.

2.2 Current mainstream cosmological observations

SN data We use the largest compilation of type Ia supernovae (SN) data in this work, which is named the Pantheon compilation [47]. The Pantheon compilation consists of 1048 SN data, which is composed of the subset of 279 SN data from the Pan-STARRS1 Medium Deep Survey in the redshift range of $0.03 < z < 0.65$ and useful distance estimates of SN from SDSS, SNLS, various low-redshift and HST samples in the redshift range of $0.01 < z < 2.3$. According to the observational point of view, using a modified version of the Tripp formula [48], in the SALT2 spectral model [49], the distance modulus can be expressed as [47]

$$\mu = m_{\rm B} - M + \alpha \times x_1 - \beta \times c + \Delta_M + \Delta_B, \qquad (7)$$

where $m_{\rm B}$, x_1, and c represent the log of the overall flux normalization, the light-curve shape parameter, and the color in the light-curve fit of SN, respectively, M repersents the absolute B-band magnitude with $x_1 = 0$ and $c = 0$ for a fiducial SN; α and β are the coefficients of the relation between luminosity and stretch and of the relation between luminosity and color, respectively. Δ_M is the distance correction from the host-galaxy mass of the SN, and Δ_B is the distance correction from predicted biases of simulations.

The luminosity distance $d_{\rm L}$ to a supernova can be given by

$$d_{\rm L}(z) = \frac{1+z}{H_0}\int_0^z \frac{{\rm d}z'}{E(z')}, \qquad (8)$$

where $E(z) = H(z)/H_0$. Note that we consider a flat universe throughout this work. The χ^2 function for SN observation is expressed as

$$\chi^2_{\rm SN} = (\mu - \mu_{\rm th})^\dagger C_{\rm SN}^{-1}(\mu - \mu_{\rm th}), \qquad (9)$$

where $C_{\rm SN}$ is the covariance matrix of the SN observation [47], and the theoretical distance modulus $\mu_{\rm th}$ is given by

$$\mu_{\rm th} = 5\log_{10}\frac{d_{\rm L}}{10{\rm pc}}. \qquad (10)$$

CMB data For the cosmic microwave background (CMB) anisotropy data, we use the "Planck distance priors" from the Planck 2015 data [50]. The distance priors include the shift parameter R, the "acoustic scale" $\ell_{\rm A}$, and the baryon density $\omega_{\rm b}$, defined by

$$R \equiv \sqrt{\Omega_{\rm m} H_0^2}(1 + z_*)D_{\rm A}(z_*), \qquad (11)$$

$$\ell_{\rm A} \equiv (1 + z_*)\frac{\pi D_{\rm A}(z_*)}{r_{\rm s}(z_*)}, \qquad (12)$$

$$\omega_{\rm b} \equiv \Omega_{\rm b}h^2, \qquad (13)$$

where $\Omega_{\rm m}$ is the present-day fractional matter density, and $D_{\rm A}(z_*)$ denotes the angular diameter distance at z_* with z_* being the redshift of the decoupling epoch of photons. In a flat universe, $D_{\rm A}$ can be expressed as

$$D_{\rm A}(z) = \frac{1}{H_0(1+z)}\int_0^z \frac{{\rm d}z'}{E(z')}, \qquad (14)$$

and $r_{\rm s}(a)$ is given by

$$r_{\rm s}(a) = \frac{1}{\sqrt{3}}\int_0^a \frac{{\rm d}a'}{a'H(a')\sqrt{1 + (3\Omega_{\rm b}/4\Omega_\gamma)a'}}, \qquad (15)$$

where $\Omega_{\rm b}$ and Ω_γ are the present-day energy densities of baryons and photons, respectively. In this work, we adopt $3\Omega_{\rm b}/4\Omega_\gamma = 31{,}500\Omega_{\rm b}h^2(T_{\rm cmb}/2.7{\rm K})^{-4}$ and $T_{\rm cmb} = 2.7255$ K. z_* can be calculated by the fitting formula [51],

$$z_* = 1048\left[1 + 0.00124\left(\Omega_{\rm b}h^2\right)^{-0.738}\right]\left[1 + g_1\left(\Omega_{\rm m}h^2\right)^{g_2}\right], \qquad (16)$$

where

$$g_1 = \frac{0.0783(\Omega_{\rm b}h^2)^{-0.238}}{1 + 39.5(\Omega_{\rm b}h^2)^{-0.76}}, \quad g_2 = \frac{0.560}{1 + 21.1(\Omega_{\rm b}h^2)^{1.81}}. \qquad (17)$$

The three values can be obtained from the Planck TT + LowP data [50]: $R = 1.7488 \pm 0.0074$, $\ell_{\rm A} = 301.76 \pm 0.14$, and $\omega_b = 0.02228 \pm 0.00023$. The χ^2 function for CMB is

$$\chi^2_{\rm CMB} = \Delta p_i[{\rm Cov}_{\rm CMB}^{-1}(p_i, p_j)]\Delta p_j, \quad \Delta p_i = p_i^{\rm th} - p_i^{\rm obs}, \qquad (18)$$

where $p_1 = R$, $p_2 = \ell_A$, $p_3 = \omega_b$, and $\text{Cov}_{\text{CMB}}^{-1}$ is the inverse covariance matrix and can be found in Ref. [50].

BAO data From the baryon acoustic oscillation (BAO) measurements, we can obtain the distance ratio $D_V(z)/r_s(z_d)$ at the effective redshift. The spherical average gives the expression of $D_V(z)$,

$$D_V(z) \equiv \left[D_M^2(z) \frac{z}{H(z)} \right]^{1/3}, \qquad (19)$$

where $D_M(z) = (1+z)D_A(z)$ is the comoving angular diameter distance [52]. $r_s(z_d)$ is the comoving sound horizon size at the redshift z_d of the drag epoch and its calculated value is given by Eq. (15). z_d is given by the fitting formula [51],

$$z_d = \frac{1291(\Omega_m h^2)^{0.251}}{1 + 0.659(\Omega_m h^2)^{0.828}} \left[1 + b_1(\Omega_b h^2)^{b_2} \right], \qquad (20)$$

with

$$b_1 = 0.313(\Omega_m h^2)^{-0.419} \left[1 + 0.607(\Omega_m h^2)^{0.674} \right],$$
$$b_2 = 0.238(\Omega_m h^2)^{0.223}. \qquad (21)$$

We use five BAO data points form the 6dF Galaxy Survey at $z_{\text{eff}} = 0.106$ [53], the SDSS-DR7 at $z_{\text{eff}} = 0.15$ [54], and the BOSS-DR12 at $z_{\text{eff}} = 0.38$, $z_{\text{eff}} = 0.51$, and $z_{\text{eff}} = 0.61$ [52]. The data used in this work from various surveys are shown in Table 1.

The χ^2 function for the BAO measurements is

$$\chi_{\text{BAO}}^2 = \sum_{i=1}^{5} \frac{\left(\xi_i^{\text{obs}} - \xi_i^{\text{th}} \right)^2}{\sigma_i^2}, \qquad (22)$$

where ξ_{th} and ξ_{obs} represent the theoretically predicted value and the experimentally measured value of the ith data point for the BAO observations, respectively, and σ_i is the standard deviation of the ith data point.

2.3 Redshift-drift observations from E-ELT and SKA

The actual measurement for the SL-test signal is the shift in the spectroscopic velocity (Δv) for a source in a given time interval (Δt_o). The spectroscopic velocity shift is usually expressed as [2]

$$\Delta v = \frac{\Delta z}{1 + z} = H_0 \Delta t_o \left[1 - \frac{E(z)}{1 + z} \right], \qquad (23)$$

where $E(z)$ is determined by a specific cosmological model.

The measurement of the velocity shift will be achieved by the upcoming experiments such as the E-ELT and SKA through two different means. The E-ELT will be able to observe the Lyman-α absorption lines of distant quasar systems to achieve the measurement of Δv in the redshift range of $z \in [2, 5]$ [2,55]. The SKA will measure the spectroscopic velocity shift Δv by observing the neutral hydrogen emission signals of galaxies at the precision of one percent in the redshift range of $z \in [0, 1]$. Obviously, the E-ELT and SKA experiments will be the ideal complements with each other, because of the explorations of different periods for the cosmic evolution.

E-ELT mock data For the E-ELT data, as discussed in Ref. [6], the standard deviation on Δv can be estimated as

$$\sigma_{\Delta v} = 1.35 \left(\frac{2370}{S/N} \right) \left(\frac{N_{\text{QSO}}}{30} \right)^{-1/2} \left(\frac{1 + z_{\text{QSO}}}{5} \right)^x \text{ cm s}^{-1}, \qquad (24)$$

where S/N is the signal-to-noise ratio of the Lyman-α spectrum, N_{QSO} is the number of observed quasars at the effective redshift z_{QSO}, and x is 1.7 for $2 \leq z \leq 4$ and 0.9 for $z \geq 4$. In this work, we assume $S/N = 3000$ and $N_{\text{QSO}} = 30$. We generate 30 mock data with a uniform distribution for the E-ELT redshift-drift observation in six redshift bins (the redshift interval is $\Delta z = 0.5$ for each bin), and we assume an observation time of $\Delta t_o = 10$ years.

SKA mock data For the case of SKA, we follow the prescription given in Refs. [56,57] to produce the mock data of redshift drift. It is shown in Refs. [56,57] that if SKA could have the full sensitivity and detect a billion galaxies, the evolution of the frequency shift in redshift space would be estimated to a precision of one percent. Thus, we consider the following two scenarios:

1. For SKA Phase 1, in our simulation, we produce 3 mock data of the drift Δv in redshift $0 < z < 0.3$ with velocity

Table 1 The BAO measurements from the various surveys used in this work. The value of $r_{s,\text{fid}} = 147.78$ Mpc is for the sound horizon for the fiducial model. Note that, for the measurements from BOSS-DR12, the first error is the statistical uncertainty, while the second value is the systematic error

z	Measurement	Experiment	References
0.106	$D_V(z)/r_s(z_d) = 2.976 \pm 0.133$	6dFGS	[53]
0.15	$D_V(z)/r_s(z_d) = 4.466 \pm 0.168$	SDSS-DR7	[54]
0.38	$D_M(z)(r_{s,\text{fid}}/r_s(z_d)) = 1512 \pm 27 \pm 14$	BOSS-DR12	[52]
0.38	$H(z)(r_{s,\text{fid}}/r_s(z_d)) = 81.2 \pm 2.2 \pm 1.0$	BOSS-DR12	[52]
0.51	$D_M(z)(r_{s,\text{fid}}/r_s(z_d)) = 1975 \pm 27 \pm 14$	BOSS-DR12	[52]
0.51	$H(z)(r_{s,\text{fid}}/r_s(z_d)) = 90.9 \pm 2.1 \pm 1.1$	BOSS-DR12	[52]
0.61	$D_M(z)(r_{s,\text{fid}}/r_s(z_d)) = 2307 \pm 33 \pm 17$	BOSS-DR12	[52]
0.61	$H(z)(r_{s,\text{fid}}/r_s(z_d)) = 99.0 \pm 2.2 \pm 1.2$	BOSS-DR12	[52]
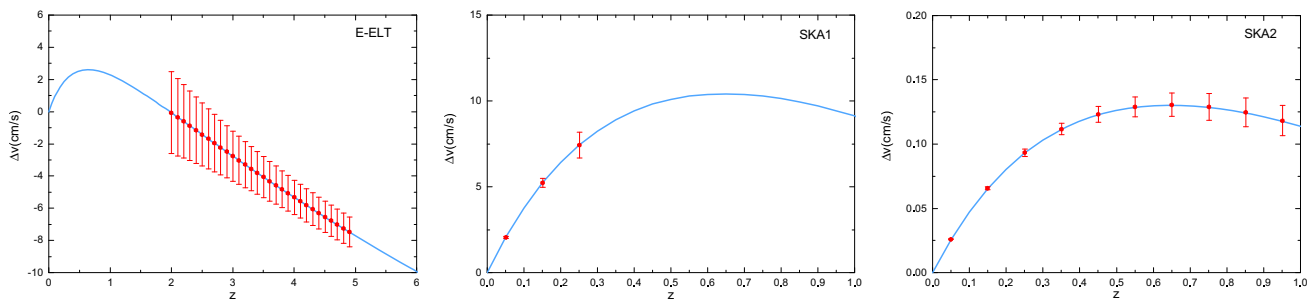
Fig. 1 Curve of Δv versus z in the ΛCDM model. Parameter values are fixed as the best-fit values to SN+CMB+BAO. The error bars on the curves are estimated from E-ELT (left), SKA1 (middle) and SKA2 (right)

uncertainties $\sigma_{\Delta v}$, respectively, of 3% in the first bin, 5% in the second bin and 10% in the third bin. The redshift interval Δz is 0.1 for each bin and the timespan Δt_o is 40 years. Note that although a timespan of 40 years is a long integration time, it can be thought of as a benchmark scenario to improve sensitivity and redshift coverage in the full SKA configuration.

2. For SKA Phase 2, we generate 10 mock data of the drift Δv in the redshift $0 < z < 1$ with the velocity uncertainty $\sigma_{\Delta v}/\Delta v$ (relative error) ranging from 1 to 10%. Here, we adopt the same treatment method for the uncertainty as in Ref. [57], i.e., the relative error $\sigma_{\Delta v}/\Delta v$ is assumed to be linearly increased from 1 to 10% in the redshift range of $z \in [0, 1]$ (from low to high redshifts). To be more specific, the relative error is assumed to be 1% in the first bin, 2% in the second bin, and so forth. This could be reached in the timespan $\Delta t_o = 0.5$ years, which leads to an extremely competitive and ideal scenario. Note that the requirement of this scenario is 10^7 galaxies observed in each bin [57].

In addition, in the mock data simulation, we adopt the scheme accordant with our previous papers [7,11–15,17]. In other words, the fiducial cosmology for the SL simulated data from E-ELT or SKA is chosen to be the best-fit cosmology according to the analysis of the data combination of SN+CMB+BAO in ΛCDM model, wCDM model, CPL model, and HDE model, respectively.

3 Results and discussion

Since the ΛCDM model is widely regarded as a prototype of standard cosmology, we take this model as a reference model to test the constraining power of the SKA-only mock data and make an analysis of constraints on cosmological parameters when the redshift-drift data of SKA and E-ELT are combined. In Fig. 1, we show the simulated redshift-drift data for E-ELT, SKA1, and SKA2, using the ΛCDM model as the fiducial model. In this figure, the curve of $\Delta v(z)$ is plotted according
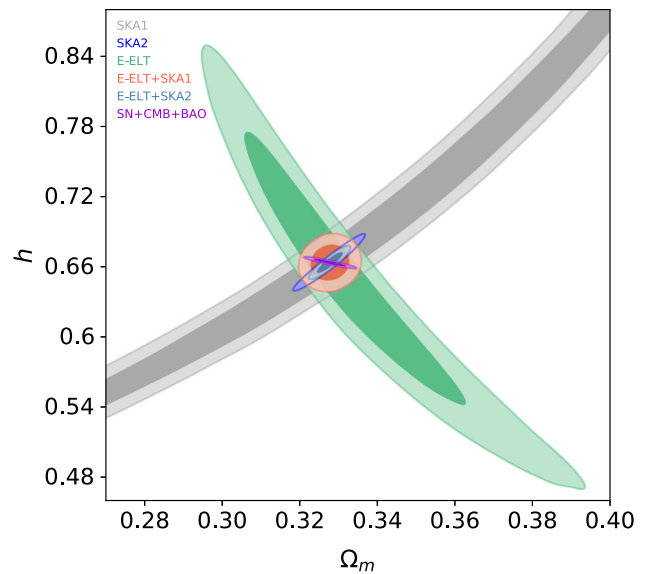
Fig. 2 Constraints (1σ and 2σ CL) on the ΛCDM model in Ω_m–h plane by using the SKA1, SKA2, E-ELT, E-ELT+SKA1, E-ELT+SKA2, and SN+CMB+BAO data

to Eq. (23), with the fiducial values of parameters given by the best fit to the SN+CMB+BAO data; the error bars on Δv, i.e., $\sigma_{\Delta v}$, for each redshift bin, are plotted according to Eq. (24) for E-ELT, and according to the detailed prescriptions described in the above section (the part entitled "SKA mock data") for SKA1 and SKA2. We find that in the E-ELT case the error of Δv decreases with the increase of redshift, and it is opposed in the SKA1 case or the SKA2 case. In Fig. 2, we plot the two-dimensional posterior contours at 68% and 95% confidence level (CL) in the ΛCDM model. We clearly see that using the SKA1-only mock data, the ΛCDM model can only be loosely constrained, while the model can be well constrained using the SKA2-only mock data.

In addition, from Fig. 2, we clearly see that in the ΛCDM model, from the E-ELT, Ω_m and h are in strong anti-correlation, while constraints from SKA1 or SKA2 provide a positive correlation for Ω_m and h, and thus the orthogonality of the two degeneracy orientations leads to a complete break-
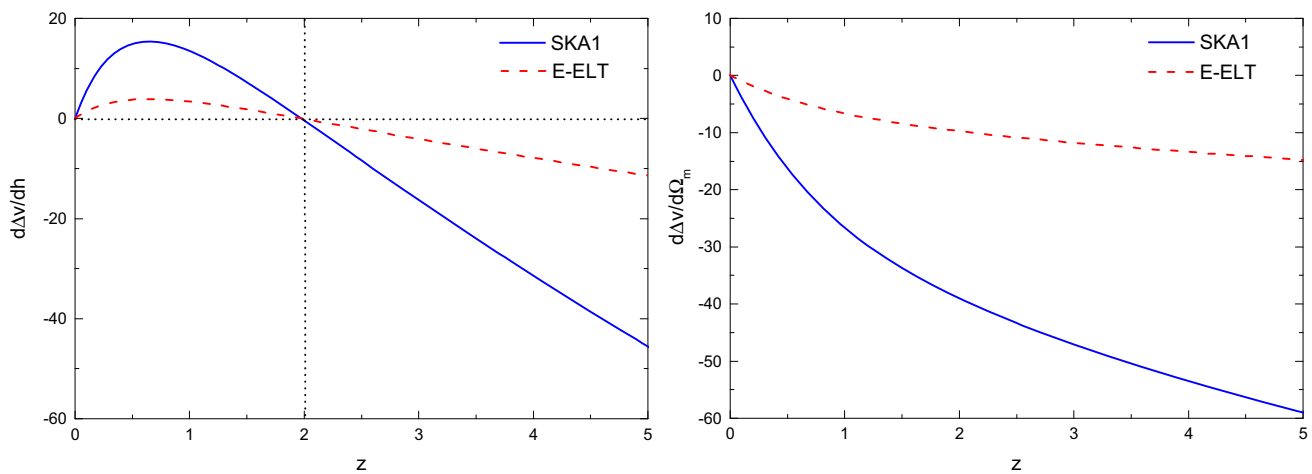
Fig. 3 Curves of $d\Delta v/dh$ versus z (left) and $d\Delta v/d\Omega_m$ versus z (right) for E-ELT and SKA in the ΛCDM model. Parameter values are set as in Fig. 1

ing for the parameter degeneracy. Thus, the constraints from the combination of E-ELT and SKA (SKA1 or SKA2) would have a tremendous improvement, as shown by the gray and red contours in Fig. 2. Particularly, the result from the combination of E-ELT+SKA2 is almost as good as the constraint from the combination of SN+CMB+BAO, which implies that the redshift-drift observation might be one of the most competitive cosmological probes. This may be due to the fact that the experiments of E-ELT and SKA are complementary in mapping the expansion history of the universe with a model-independent way. That is to say, these two experiments will be able to directly perform a reconstruction of the expansion history of the universe in the dark matter- or dark energy-dominated epochs by using different observational techniques.

In order to understand why Ω_m and h are in positive correlation for SKA and in anti-correlation for E-ELT, we make a deeper analysis by a comparison of the curves of derivatives of Δv with respect to Ω_m and h versus z for E-ELT and SKA. The curves of $d\Delta v/dh$ and $d\Delta v/d\Omega_m$ versus z are shown in Fig. 3. We find that $d\Delta v/d\Omega_m$ always decreases with increased z, i.e., the varying tendencies of $d\Delta v/d\Omega_m$ for E-ELT and SKA are the same though the values of $d\Delta v/d\Omega_m$ are not the same. However, $d\Delta v/dh$ is increasing in most of the SKA redshift range of $z \in [0, 1]$ (roughly the range of $z \lesssim 0.6$, covering the whole range of SKA Phase 1), and it is decreasing in the E-ELT redshift range of $z \in [2, 5]$. Meanwhile, $d\Delta v/dh$ is positive in the SKA redshift range of $z \in [0, 1]$, and it is negative in the E-ELT redshift range of $z \in [2, 5]$. The two experiments are therefore complementary in this sense, and we can clearly understand why the degeneracies between Ω_m and h can be well broken by the two experiments, as shown in Fig. 2. Notice that in Fig. 3 the blue solid curves of $d\Delta v/dh$ and $d\Delta v/d\Omega_m$ are plotted for

Table 2 Priors on the free parameters for the ΛCDM, wCDM, CPL, and HDE models in a flat universe

Parameters	Prior
$\Omega_b h^2$	[0.005, 0.100]
$\Omega_c h^2$	[0.001, 0.990]
w_0	[−3.000, 1.000]
w_a	[−14.000, 7.000]
c	[0.200, 1.200]

SKA1. We do not show the case of SKA2, since the coordinate proportions are too different, which is due to a small timespan Δt_o in the SAK2 simulation.

Meanwhile, we find that the degeneracy orientation of E-ELT+SKA1 or E-ELT+SKA2 in the parameter plane is evidently different from result for the combination of SN+CMB+BAO. This phenomenon would result in an effective breaking of the parameter degeneracy and a significant improvement of the constraints on dark energy. It is of extreme interest to know what role the redshift-drift data of SKA will play in constraining dark energy in the future. Next we will explore this issue in detail.

We constrain the ΛCDM, wCDM, CPL and HDE models by using the data combinations of SN+CMB+BAO, SN+CMB+BAO+E-ELT, SN+CMB+BAO+E-ELT+SKA1, and SN+CMB+BAO+E-ELT+SKA2 to complete our analysis. The priors of the free parameters are given in Table 2. Here, $\Omega_b h^2$ and $\Omega_c h^2$, respectively, stand for the physical baryon and cold dark matter densities. The constraint results are presented in Tables 3, 4, 5 and Figs. 4, 5. In Table 3, we show the best-fit results with the 1σ errors quoted. The constraint errors and precisions of the cosmological parameters are given in Tables 4 and 5, respectively. Here, for a parameter ξ, we use $\sigma(\xi)$ to denote its 1σ error. For the cases that its

Table 3 Fitting results of parameters in the ΛCDM, wCDM, CPL, and HDE models using SN+CMB+BAO, SN+CMB+BAO+E-ELT, SN+CMB+BAO+E-ELT+SKA1, and SN+CMB+BAO+E-ELT+SKA2

Data	SN+CMB+BAO				SN+CMB+BAO+E-ELT			
Model	ΛCDM	wCDM	CPL	HDE	ΛCDM	wCDM	CPL	HDE
w_0	–	$-1.0176^{+0.0395}_{-0.0435}$	$-1.0416^{+0.0919}_{-0.0937}$	–	–	$-1.0191^{+0.0391}_{-0.0391}$	$-1.0373^{+0.0805}_{-0.0865}$	–
w_a	–	–	$0.1141^{+0.3248}_{-0.3860}$	–	–	–	$0.0933^{+0.3289}_{-0.3482}$	–
c	–	–	–	$0.6651^{+0.0397}_{-0.0378}$	–	–	–	$0.6658^{+0.0363}_{-0.0344}$
$\Omega_{\rm m}$	$0.3097^{+0.0072}_{-0.0068}$	$0.3082^{+0.0078}_{-0.0084}$	$0.3077^{+0.0081}_{-0.0090}$	$0.3018^{+0.0081}_{-0.0081}$	$0.3097^{+0.0048}_{-0.0048}$	$0.3080^{+0.0054}_{-0.0050}$	$0.3076^{+0.0053}_{-0.0053}$	$0.3023^{+0.0050}_{-0.0050}$
h	$0.6772^{+0.0052}_{-0.0053}$	$0.6800^{+0.0093}_{-0.0084}$	$0.6798^{+0.0096}_{-0.0081}$	$0.6794^{+0.0091}_{-0.0097}$	$0.6771^{+0.0037}_{-0.0037}$	$0.6803^{+0.0064}_{-0.0068}$	$0.6800^{+0.0068}_{-0.0067}$	$0.6790^{+0.0060}_{-0.0059}$
Data	SN+CMB+BAO				SN+CMB+BAO+E-ELT			
Model	ΛCDM	wCDM	CPL	HDE	ΛCDM	wCDM	CPL	HDE
w_0	–	$-1.0189^{+0.0361}_{-0.0358}$	$-1.0396^{+0.0810}_{-0.0822}$	–	–	$-1.0174^{+0.0309}_{-0.0324}$	$-1.0395^{+0.0791}_{-0.0798}$	–
w_a	–	–	$0.1012^{+0.3153}_{-0.3629}$	–	–	–	$0.0986^{+0.3206}_{-0.3515}$	–
c	–	–	–	$0.6607^{+0.0169}_{-0.0149}$	–	–	–	$0.6613^{+0.0105}_{-0.0110}$
$\Omega_{\rm m}$	$0.3097^{+0.0040}_{-0.0039}$	$0.3083^{+0.0038}_{-0.0041}$	$0.3076^{+0.0039}_{-0.0040}$	$0.3019^{+0.0043}_{-0.0044}$	$0.3096^{+0.0013}_{-0.0013}$	$0.3083^{+0.0015}_{-0.0015}$	$0.3077^{+0.0016}_{-0.0016}$	$0.3018^{+0.0038}_{-0.0036}$
h	$0.6772^{+0.0030}_{-0.0030}$	$0.6801^{+0.0052}_{-0.0052}$	$0.6799^{+0.0054}_{-0.0054}$	$0.6797^{+0.0032}_{-0.0032}$	$0.6772^{+0.0012}_{-0.0012}$	$0.6800^{+0.0027}_{-0.0027}$	$0.6798^{+0.0031}_{-0.0032}$	$0.6798^{+0.0023}_{-0.0024}$

Table 4 Constraint errors of parameters in the ΛCDM, wCDM, CPL, and HDE models using SN+CMB+BAO, SN+CMB+BAO+E-ELT, SN+CMB+BAO+E-ELT+SKA1, and SN+CMB+BAO+E-ELT+SKA2

Data	SN+CMB+BAO				SN+CMB+BAO+E-ELT			
Model	ΛCDM	wCDM	CPL	HDE	ΛCDM	wCDM	CPL	HDE
$\sigma(w_0)$	–	0.0415	0.0928	–	–	0.0391	0.0835	–
$\sigma(w_a)$	–	–	0.3554	–	–	–	0.3385	–
$\sigma(c)$	–	–	–	0.0388	–	–	–	0.0353
$\sigma(\Omega_{\rm m})$	0.0071	0.0081	0.0086	0.0081	0.0048	0.0052	0.0053	0.0050
$\sigma(h)$	0.0053	0.0089	0.0089	0.0094	0.0037	0.0066	0.0068	0.0060
Data	SN+CMB+BAO				SN+CMB+BAO+E-ELT			
Model	ΛCDM	wCDM	CPL	HDE	ΛCDM	wCDM	CPL	HDE
$\sigma(w_0)$	–	0.0360	0.0816	–	–	0.0317	0.0795	–
$\sigma(w_a)$	–	–	0.3391	–	–	–	0.3361	–
$\sigma(c)$	–	–	–	0.0159	–	–	–	0.0108
$\sigma(\Omega_{\rm m})$	0.0040	0.0040	0.0040	0.0044	0.0013	0.0015	0.0016	0.0037
$\sigma(h)$	0.0030	0.0052	0.0054	0.0032	0.0012	0.0027	0.0032	0.0024

distribution slightly deviates from the gaussian distribution, we adopt the value of averaging the upper-limit and lower-limit errors. We use $\varepsilon(\xi) = \sigma(\xi)/\xi_{\rm bf}$ to denote the relative error of the parameter ξ, where $\xi_{\rm bf}$ is its best-fit value. In this paper, for convenience, we also informally call $\varepsilon(\xi)$ the "constraint precision" of the parameter ξ. Note that we do not calculate the constraint precision for the parameter w_a, since its central value is close to 0. In Figs. 4 and 5, we show the two-dimensional posterior distribution contours of con-

straint results in the ΛCDM, wCDM, CPL and HDE models at the 68% and 95% CL.

From these figures, we clearly see that when the E-ELT mock data are combined with SN+CMB+BAO, the parameter spaces can be significantly reduced in the ΛCDM, wCDM, and HDE models, while there is little significant improvement in the parameter space for the CPL model. Adding the SKA1 mock data to the data combination of SN+CMB+BAO+E-ELT, the parameter spaces are sharply reduced. In particular, when the SKA2 mock data

Table 5 Constraint precisions of parameters in ΛCDM, wCDM, CPL, and HDE models using SN+CMB+BAO, SN+CMB+BAO+E-ELT, SN+CMB+BAO+E-ELT+SKA1, and SN+CMB+BAO+E-ELT+SKA2

Data	SN+CMB+BAO				SN+CMB+BAO+E-ELT			
Model	ΛCDM	wCDM	CPL	HDE	ΛCDM	wCDM	CPL	HDE
$\varepsilon(w_0)$	–	0.0408	0.0891	–	–	0.0384	0.0805	–
$\varepsilon(c)$	–	–	–	0.0583	–	–	–	0.0530
$\varepsilon(\Omega_m)$	0.0229	0.0262	0.0279	0.0268	0.0155	0.0169	0.0172	0.0165
$\varepsilon(h)$	0.0078	0.0131	0.0130	0.0138	0.0054	0.0097	0.0100	0.0088
Data	SN+CMB+BAO				SN+CMB+BAO+E-ELT			
Model	ΛCDM	wCDM	CPL	HDE	ΛCDM	wCDM	CPL	HDE
$\varepsilon(w_0)$	–	0.0353	0.0785	–	–	0.0312	0.0765	–
$\varepsilon(c)$	–	–	–	0.0241	–	–	–	0.0163
$\varepsilon(\Omega_m)$	0.0129	0.0128	0.0130	0.0146	0.0042	0.0049	0.0051	0.0123
$\varepsilon(h)$	0.0044	0.0076	0.0079	0.0047	0.0018	0.0040	0.0047	0.0035

are combined with SN+CMB+BAO+E-ELT, the improvement is actually much more significant than the case of SN+CMB+BAO+E-ELT+SKA1. Meanwhile, from Fig. 5, we can easily find that the E-ELT and SKA mock data can help to break the parameter degeneracies, in particular between the parameters Ω_m and c in the HDE model.

From Table 5, we can easily find that the E-ELT, SKA1, and SKA2 can significantly improve the constraints on almost all the parameters to different extent, in particular for SKA2. Concretely, when the E-ELT mock data are combined with SN+CMB+BAO, the precision of Ω_m is improved from 2.29 to 1.55% in the ΛCDM model, from 2.62 to 1.69% in the wCDM model, from 2.79 to 1.72% in the CPL model, from 2.68 to 1.65% in the HDE model. The precisions of h, w_0, and c are also enhanced in the ΛCDM, wCDM, CPL, and HDE models; for details, see Table 5. Adding the SKA1 mock data to the data combination of SN+CMB+BAO+E-ELT, the improvement of the constraint on parameter Ω_m is from 1.55 to 1.29% in the ΛCDM model, from 1.69 to 1.28% in the wCDM model, from 1.72 to 1.30% in the CPL model, and from 1.65 to 1.46% in the HDE model. For the parameter h, the constraint is improved from 0.54 to 0.44% in the ΛCDM model, from 0.97 to 0.76% in the wCDM model, from 1.00 to 0.79% in the CPL model, and from 0.88 to 0.47%. For the parameters of dark energy, the improvement is from 3.84 to 3.53% for the parameter w in the wCDM model, from 8.05 to 7.85% for the parameter w_0 in the CPL model, and from 5.30 to 2.41% for the parameter c in the HDE model.

Furthermore, when the SKA2 mock data are combined with SN+CMB+BAO+E-ELT, the improvement of the constraint on the parameter Ω_m is from 1.55 to 0.42% in the ΛCDM model, from 1.69 to 0.49% in the wCDM model, from 1.72 to 0.51% in the CPL model, and from 1.65 to

1.23% in the HDE model. For the parameter h, the constraint is improved from 0.54 to 0.18% in the ΛCDM model, from 0.97 to 0.40% in the wCDM model, from 1.00 to 0.47% in the CPL model, and from 0.88 to 0.35% in the HDE model. For the parameters of dark energy, the improvement is from 3.84 to 3.12% for the parameter w in the wCDM model, from 8.05 to 7.65% for the parameter w_0 in the CPL model, and from 5.30 to 1.63% for the parameter c in the HDE model. We also see that for the CPL model the error of w_a is reduced by 0.74% once the SKA2 data are considered. Therefore, we conclude that the redshift-drift data of SKA will help to significantly improve the constraints of parameters and break the degeneracy between the parameters in constraining dark energy in the future.

4 Conclusion

In this work, we wish to investigate to what extent the cosmological parameters can be constrained when the redshift-drift data of SKA are used and what will happen when the combination of SKA and E-ELT mock data is considered. We use the five data sets, i.e., SKA1, SKA2, E-ELT, E-ELT+SKA1, E-ELT+SKA2, and SN+CMB+BAO to reach our aims in the ΛCDM model. We find that using the SKA2 mock data alone, the ΛCDM model can be constrained well, while the constraint is weak from the mock data of SKA1-only. When the redshift-drift mock data of SKA and E-ELT are combined, the results show that the parameter space is dramatically reduced, becoming almost as good as SN+CMB+BAO. Thus, the last aim of this work is to investigate what role the redshift-drift data of SKA will play in constraining dark energy in the future. To fulfill the task, we employ several
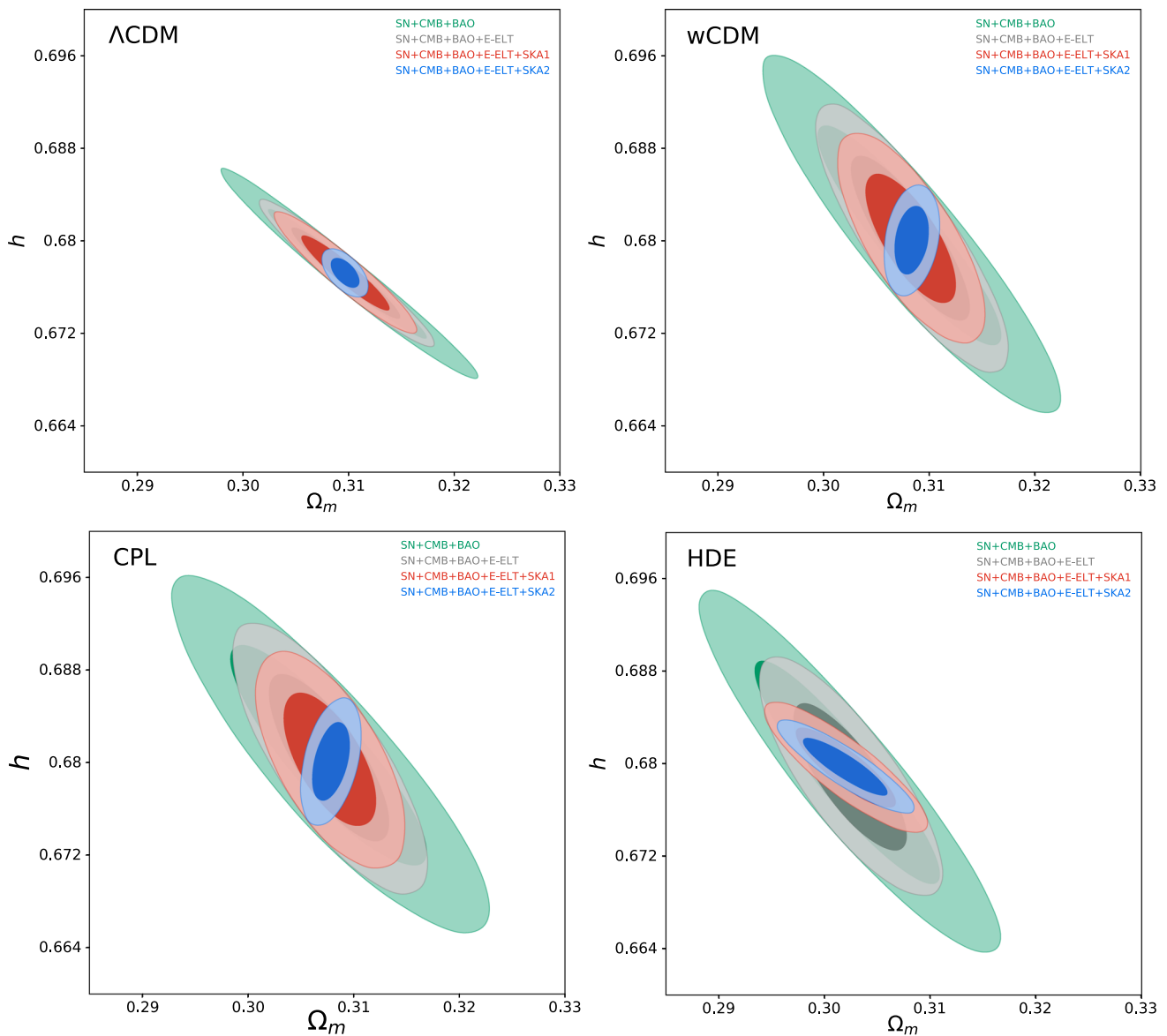
Fig. 4 Constraints (1σ and 2σ CL) on ΛCDM, wCDM, CPL, and HDE models from the SN+CMB+BAO, SN+CMB+BAO+E-ELT, SN+CMB+BAO+E-ELT+SKA1, and SN+CMB+BAO+E-ELT+SKA2 data in the Ω_m–h plane

concrete dark energy models, including the ΛCDM, wCDM, CPL, and HDE models, which are still consistent with the current observations at least to some extent.

We first use the data combination of SN+CMB+BAO to constrain the four dark energy models, and then we consider the addition of the E-ELT mock data in the data combination, i.e., we use the data combination of SN+CMB+BAO+E-ELT to constrain the models. The constraints on cosmological parameters are tremendously improved for the ΛCDM, wCDM, and HDE models, while E-ELT mock data do not help improve constraints in the CPL model. When adding the SKA1 mock data to the SN+CMB+BAO+E-ELT, the constraint results are significantly improved in all the four dark

energy models. For example, with the help of the SKA1 mock data, the constraints on Ω_m are improved by 10–25%, and the constraints on h are improved by 15–50%. Furthermore, when the SKA2 mock data are combined with the data set of SN+CMB+BAO+E-ELT, the constraint results are tremendously improved in all the four dark energy models. Concretely, the constraints on Ω_m are improved by 25–70%, and the constraints on h are improved by 50–70%. We also find that the degeneracy between cosmological parameters could be effectively broken by the combination of the E-ELT and SKA mock data. Therefore, we can conclude that in the future the redshift-drift observation of SKA would help to improve the constraints in constraining dark energy and have a high
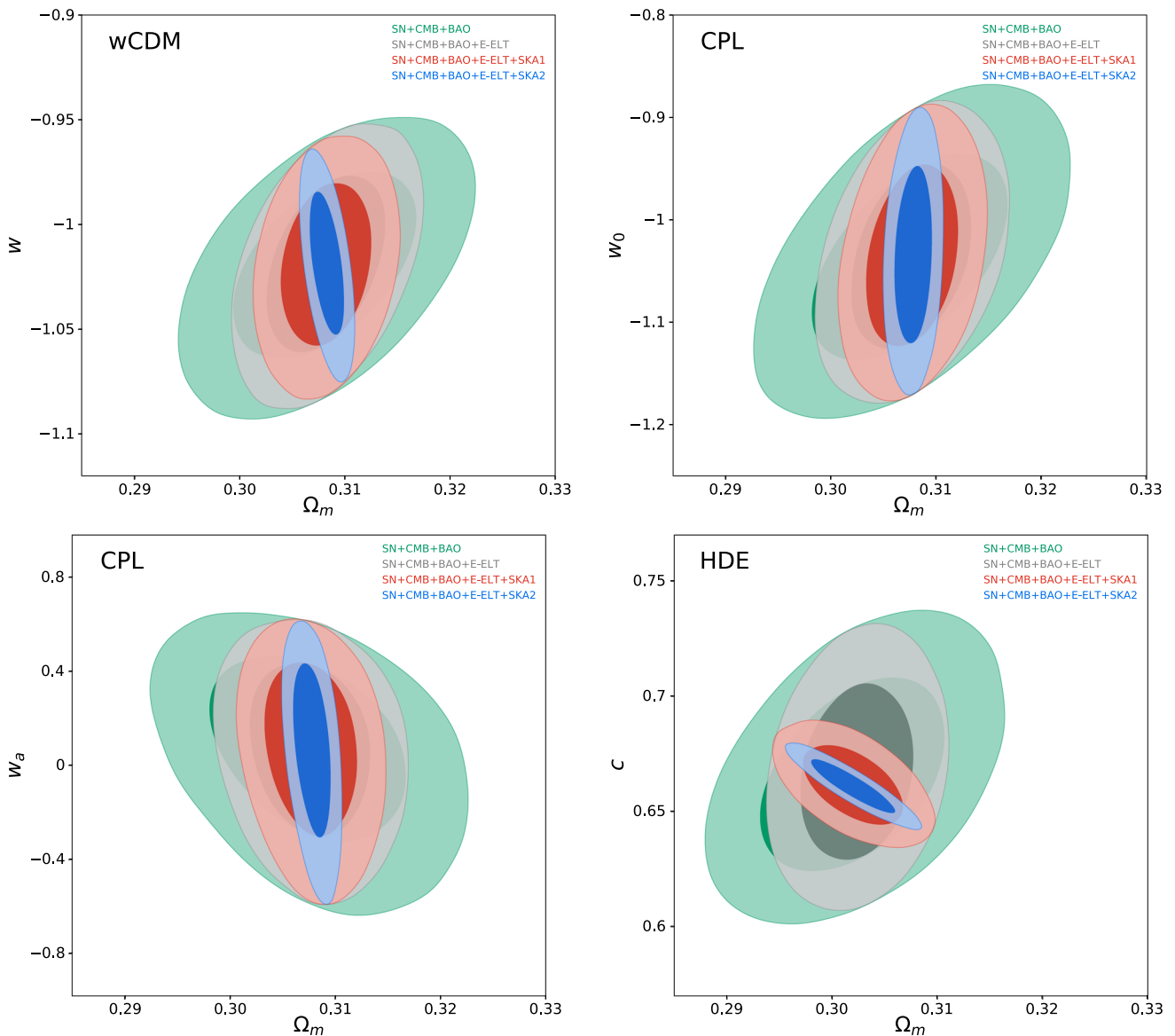
Fig. 5 Constraints (1σ and 2σ CL) in the $\Omega_{\mathrm{m}}-w$ plane for wCDM model, in the $\Omega_{\mathrm{m}}-w_0$ plane for CPL model, in the $\Omega_{\mathrm{m}}-w_a$ plane for CPL model, and in the $\Omega_{\mathrm{m}}-c$ plane for HDE model from the SN+CMB+BAO, SN+CMB+BAO+E-ELT, SN+CMB+BAO+E-ELT+SKA1, and SN+CMB+BAO+E-ELT+SKA2 data

potential to be one of the most competitive cosmological probes in constraining dark energy.

Data Availability Statement This manuscript has no associated data or the data will not be deposited. [Authors' comment: This is a theoretical study. In this work, we use some public observational data to constrain theoretical models, which does not yield associated experimental data.]

References

1. A. Sandage, Astrophys. J. **136**, 319 (1962)
2. A. Loeb, Astrophys. J. **499**, L111 (1998). arXiv:astro-ph/9802122
3. H.B. Zhang, W.H. Zhong, Z.H. Zhu, S. He, Phys. Rev. D **76**, 123508 (2007). arXiv:0705.4409 [astro-ph]
4. P.S. Corasaniti, D. Huterer, A. Melchiorri, Phys. Rev. D **75**, 062001 (2007). arXiv:astro-ph/0701433
5. A. Balbi, C. Quercellini, Mon. Not. R. Astron. Soc. **382**, 1623 (2007). arXiv:0704.2350 [astro-ph]
6. J. Liske et al., Mon. Not. Roy. Astron. Soc. **386**, 1192 (2008). arXiv:0802.1532 [astro-ph]
7. J. Zhang, L. Zhang, X. Zhang, Phys. Lett. B **691**, 11 (2010). arXiv:1006.1738 [astro-ph.CO]
8. M. Martinelli et al., Phys. Rev. D **86**, 123001 (2012). arXiv:1210.7166 [astro-ph.CO]
9. S. Yuan, T.J. Zhang, JCAP **1502**(02), 025 (2015). arXiv:1311.1583 [astro-ph.CO]
10. M.J. Zhang, W.B. Liu, arXiv:1311.6858 [astro-ph.CO]
11. J.J. Geng, J.F. Zhang, X. Zhang, JCAP **1407**, 006 (2014). arXiv:1404.5407 [astro-ph.CO]
12. J.J. Geng, J.F. Zhang, X. Zhang, JCAP **1412**(12), 018 (2014). [arXiv:1407.7123 [astro-ph.CO]]
13. J.J. Geng, Y.H. Li, J.F. Zhang, X. Zhang, Eur. Phys. J. C **75**(8), 356 (2015). arXiv:1501.03874 [astro-ph.CO]
14. R.Y. Guo, X. Zhang, Eur. Phys. J. C **76**(3), 163 (2016). arXiv:1512.07703 [astro-ph.CO]
15. D.Z. He, J.F. Zhang, X. Zhang, Sci. China Phys. Mech. Astron. **60**(3), 039511 (2017). https://doi.org/10.1007/s11433-016-0472-1. arXiv:1607.05643 [astro-ph.CO]
16. R. Lazkoz, I. Leanizbarrutia, V. Salzano, Eur. Phys. J. C **78**(1), 11 (2018). arXiv:1712.07555 [astro-ph.CO]
17. J.J. Geng, R.Y. Guo, A. Wang, J.F. Zhang, X. Zhang, Commun. Theor. Phys. **70**(4), 445 (2018). arXiv:1806.10735 [astro-ph.CO]
18. Y. Liu, R.Y. Guo, J.F. Zhang, X. Zhang, JCAP **1905**, 016 (2019). arXiv:1811.12131 [astro-ph.CO]
19. M. Chevallier, D. Polarski, Int. J. Mod. Phys. D **10**, 213 (2001). arXiv:gr-qc/0009008
20. E.V. Linder, Phys. Rev. Lett. **90**, 091301 (2003). arXiv:astro-ph/0208512
21. A.G. Cohen, D.B. Kaplan, A.E. Nelson, Phys. Rev. Lett. **82**, 4971 (1999). arXiv:hep-th/9803132
22. M. Li, Phys. Lett. B **603**, 1 (2004). arXiv:hep-th/0403127
23. X. Zhang, Int. J. Mod. Phys. D **14**, 1597 (2005). arXiv:astro-ph/0504586
24. X. Zhang, F.Q. Wu, Phys. Rev. D **72**, 043524 (2005). arXiv:astro-ph/0506310
25. X. Zhang, Phys. Rev. D **74**, 103505 (2006). https://doi.org/10.1103/PhysRevD.74.103505. arXiv:astro-ph/0609699
26. X. Zhang, Phys. Lett. B **648**, 1 (2007). https://doi.org/10.1016/j.physletb.2007.02.069. arXiv:astro-ph/0604484
27. X. Zhang, F.Q. Wu, Phys. Rev. D **76**, 023502 (2007). [arXiv:astro-ph/0701405]
28. J. Zhang, X. Zhang, H. Liu, Phys. Lett. B **651**, 84 (2007). https://doi.org/10.1016/j.physletb.2007.06.019. arXiv:0706.1185 [astro-ph]
29. Jf Zhang, X. Zhang, Hy Liu, Eur. Phys. J. C **52**, 693 (2007). https://doi.org/10.1140/epjc/s10052-007-0408-2. arXiv:0708.3121 [hep-th]
30. J.F. Zhang, X. Zhang, H. Liu, Eur. Phys. J. C **54**, 303 (2008). https://doi.org/10.1140/epjc/s10052-008-0532-7. arXiv:0801.2809 [astro-ph]
31. C. Gao, F. Wu, X. Chen, Y.G. Shen, Phys. Rev. D **79**, 043511 (2009). arXiv:0712.1394 [astro-ph]
32. M. Li, X.D. Li, S. Wang, X. Zhang, JCAP **0906**, 036 (2009). arXiv:0904.0928 [astro-ph.CO]
33. X. Zhang, Phys. Rev. D **79**, 103509 (2009). https://doi.org/10.1103/PhysRevD.79.103509. arXiv:0901.2262 [astro-ph.CO]
34. C.J. Feng, X. Zhang, Phys. Lett. B **680**, 399 (2009). https://doi.org/10.1016/j.physletb.2009.09.040. arXiv:0904.0045 [gr-qc]
35. M. Li, X. Li, X. Zhang, Sci. China Phys. Mech. Astron. **53**, 1631 (2010). arXiv:0912.3988 [astro-ph.CO]
36. J.L. Cui, L. Zhang, J.F. Zhang, X. Zhang, Chin. Phys. B **19**, 019802 (2010). https://doi.org/10.1088/1674-1056/19/1/019802. arXiv:0902.0716 [astro-ph.CO]
37. Y.H. Li, S. Wang, X.D. Li, X. Zhang, JCAP **1302**, 033 (2013). https://doi.org/10.1088/1475-7516/2013/02/033. arXiv:1207.6679 [astro-ph.CO]
38. J.F. Zhang, M.M. Zhao, J.L. Cui, X. Zhang, Eur. Phys. J. C **74**(11), 3178 (2014). https://doi.org/10.1140/epjc/s10052-014-3178-7. arXiv:1409.6078 [astro-ph.CO]
39. J.L. Cui, J.F. Zhang, Eur. Phys. J. C **74**, 2849 (2014). arXiv:1402.1829 [astro-ph.CO]
40. J.F. Zhang, J.L. Cui, X. Zhang, Eur. Phys. J. C **74**(10), 3100 (2014). arXiv:1409.6562 [astro-ph.CO]
41. J.F. Zhang, M.M. Zhao, Y.H. Li, X. Zhang, JCAP **1504**, 038 (2015). https://doi.org/10.1088/1475-7516/2015/04/038. arXiv:1502.04028 [astro-ph.CO]
42. X. Zhang, Phys. Rev. D **93**(8), 083011 (2016). https://doi.org/10.1103/PhysRevD.93.083011. arXiv:1511.02651 [astro-ph.CO]
43. S. Wang, Y.F. Wang, D.M. Xia, X. Zhang, Phys. Rev. D **94**(8), 083519 (2016). https://doi.org/10.1103/PhysRevD.94.083519. arXiv:1608.00672 [astro-ph.CO]
44. M.M. Zhao, D.Z. He, J.F. Zhang, X. Zhang, Phys. Rev. D **96**(4), 043520 (2017). https://doi.org/10.1103/PhysRevD.96.043520. arXiv:1703.08456 [astro-ph.CO]
45. L. Feng, Y.H. Li, F. Yu, J.F. Zhang, X. Zhang, Eur. Phys. J. C **78**(10), 865 (2018). https://doi.org/10.1140/epjc/s10052-018-6338-3. arXiv:1807.03022 [astro-ph.CO]
46. J.F. Zhang, H.Y. Dong, J.Z. Qi, X. Zhang, Eur. Phys. J. C **80**(3), 217 (2020). arXiv:1906.07504 [astro-ph.CO]
47. D.M. Scolnic et al., Astrophys. J. **859**(2), 101 (2018). arXiv:1710.00845 [astro-ph.CO]
48. R. Tripp, A&A **331**, 815 (1998)
49. SNLS Collaboration J. Guy et al. A& A **523**, A7 (2010). arXiv:1010.4743 [astro-ph.CO]
50. P.A.R. Ade et al. [Planck Collaboration], Astron. Astrophys. **594**, A14 (2016). arXiv:1502.01590 [astro-ph.CO]
51. W. Hu, N. Sugiyama, Astrophys. J. **471**, 542 (1996). arXiv:astro-ph/9510117
52. S. Alam et al. [BOSS Collaboration], Mon. Not. R. Astron. Soc. **470**(3), 2617 (2017). arXiv:1607.03155 [astro-ph.CO]
53. F. Beutler et al., Mon. Not. R. Astron. Soc. **416**, 3017 (2011). arXiv:1106.3366 [astro-ph.CO]
54. A.J. Ross, L. Samushia, C. Howlett, W.J. Percival, A. Burden, M. Manera, Mon. Not. R. Astron. Soc. **449**(1), 835 (2015). arXiv:1409.3242 [astro-ph.CO]
55. J. Liske et al., Top Level Requirements For ELT-HIRES, Document ESO 204697 Version 1 (2014)
56. H.R. Klckner et al., PoS AASKA **14**, 027 (2015). arXiv:1501.03822 [astro-ph.CO]
57. C.J.A.P. Martins, M. Martinelli, E. Calabrese, M.P.L.P. Ramos, Phys. Rev. D **94**(4), 043001 (2016). arXiv:1606.07261 [astro-ph.CO]